PAPER

CrossMark
← click for updates

Ternary transition-metal fluoride precursors for the fluorolytic sol–gel route: new insights into speciation and decomposition†

J. Kohl,[a] D. Wiedemann,*[a] S. I. Troyanov,[b] E. Palamidis[a] and M. Lerch[a]

The nanoscaled ternary transition-metal fluorides Li_3MF_6 (M = V, Fe, Mn) and Li_2NiF_4 are promising candidates for cathode materials in high-voltage lithium-ion batteries. The fluorolytic route to these compounds relies on thermal decomposition of a hitherto uncharacterised precursor mixture produced from acetylacetonates and hydrofluoric acid. By addition of pyridine, different cationic, electroneutral and anionic complexes containing the motifs $[MF_n]^{(3-n)+}$ (n = 0–4) have been trapped and characterised by single-crystal X-ray diffraction and IR spectroscopy. Based on the results, a model of successive and incomplete fluorination is proposed for the speciation and formation of the precursor. The decomposition of the latter has been monitored *via* thermogravimetry (TG) and differential scanning calorimetry (DSC).

Introduction

In search of new cathode materials for lithium-ion batteries during the last decade, ternary fluorides have become candidates of interest, because theoretical calculations had indicated an increase in redox potential when substituting fluorine for oxygen.[1] Because of their high lithium content and their variability in oxidation numbers, the ternary fluorides Li_3MF_6 (M: transition metal) are a focus of research. The preparation of nanosized particles is important with regard to fluorides exhibiting low electrical conductivity. Detailed descriptions of the syntheses and scrutinous electrochemical characterisations of Li_3FeF_6 and Li_3VF_6 are available.[2–4] In 2012, we reported an approach for the synthesis of ternary fluorides Li_3MF_6 on the basis of the fluorolytic sol–gel process developed by Kemnitz *et al.*, who described the preparation of a high-surface aluminium fluoride.[5,6] The starting materials of our route are lithium *tert*-butoxide and a transition-metal acetylacetonate $[M^{III}(acac)_3]$, which are reacted with an excess of hydrogen fluoride in an organic solvent (*cf.* Scheme 1).

The precursor obtained in this first step is then calcined in a dinitrogen atmosphere to form the ternary fluoride. Using this protocol, either modification of Li_3VF_6 can be prepared in

$$3\ LiOtBu + [V(acac)_3] \xrightarrow[\text{EtOH}]{\text{exc. HF}} \text{precursor} \xrightarrow[\substack{N_2 \\ \text{atmosphere}}]{300–600\ ^\circ C} Li_3VF_6$$
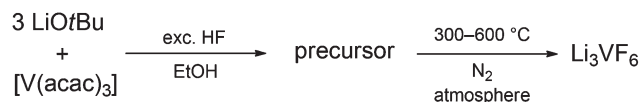
Scheme 1 Preparation of Li_3VF_6 *via* the fluorolytic sol–gel route (*t*Bu: *tert*-butyl, Et: ethyl).

excellent yield: heating of the sample to 300 °C followed by slow cooling to room temperature results in the formation of monoclinic β-Li_3VF_6, whereas heating the precursor to 700 °C and quenching to room temperature results in the formation of orthorhombic α-Li_3VF_6. Moreover, β-Li_3VF_6 can be prepared with domain sizes smaller than 50 nm. While monoclinic β-Li_3CrF_6 can be synthesised in good yield, the yields of other ternary fluorides are considerably lower—and Li_3MnF_6 as well as Li_3CoF_6 cannot at all be synthesised following this route. Monoclinic Li_3FeF_6 and Li_2MnF_5 are obtained in moderate to low yields together with the difluorides MF_2. In contrast to this, the method can be successfully applied to the system Li–Ni–F: Li_2NiF_4 is prepared in high yields with domain sizes of 55 nm.[7] The precursors contain highly amorphous fractions, making it impossible to get information about their composition by X-ray powder diffraction techniques. Only the existence of LiF and Li_2SiF_6 in the precursor materials has been confirmed so far. As shown by elemental analyses, the precursors contain high amounts of carbon, hydrogen and oxygen indicating the presence of organic residues. For example, the Li_3VF_6 precursor additionally contains acetylacetonato ligands bound to vanadium(III) as well as hexafluoridovanadate(III). This has been confirmed by IR spectroscopy and ^{1}H-NMR

[a]Technische Universität Berlin, Institut für Chemie, Straße des 17. Juni 135, 10623 Berlin, Germany. E-mail: dennis.wiedemann@chem.tu-berlin.de; Fax: +49 30 314-79656; Tel: +49 30 314-26178
[b]Humboldt-Universität zu Berlin, Institut für Chemie, Brook-Taylor-Straße 2, 12489 Berlin, Germany. E-mail: sergej.troyanov@rz.hu-berlin.de; Fax: +49 30 2093-7468; Tel: +49 30 2093-7303

spectroscopy in solution.[6] The material obtained from precursor decomposition contains about 2% residual carbon. However, it was suggested that the precursor be a mixture of several species. Accurate information about its composition is essential for optimising precursor synthesis and decomposition. Bearing this in mind, we have chosen to try and stabilise single species by providing additional donor molecules and crystallise the compounds thus obtained.[8] Using this technique, the first of a whole cascade of fluorination steps has been identified and its product, after addition of acetonitrile, $[V^{III}(acac)_2(CH_3CN)_2]BF_4$ crystallographically characterised.[6] In this work, we report on further experiments of the same kind. By addition of pyridine, we stabilised four new species in the system Li–V–F. These reflect the stepwise fluorination process of the starting material $[V^{III}(acac)_3]$, leading to $[VF_4]^-$. We have also successfully transferred this concept to Li_2MnF_5 and Li_2NiF_4 precursors.

Experimental

Analysis and characterisation

NMR spectroscopy. Liquid-phase NMR spectra were recorded on a "Bruker ARV 400" at room temperature. Chemical shifts refer to $SiMe_4$ and $VOCl_3$ for ^1H and ^{51}V, respectively. They were calibrated with respect to the solvent proton signal for ^1H or an electronically stored frequency for ^{51}V.

FT-IR spectroscopy. IR spectra of CsI pellets were measured with a "Nicolet Series II Magna 750" in transmission mode.

Elemental analysis. Carbon and hydrogen contents were determined by combustion analysis using a "Thermo Finnigan FlashEA 1112 NC" analyser. Deviations from calculated element contents result from solvent residues and difficulties in the mechanical separation of the crystalline compounds **1a**, **1b** and **1d**.

Thermal analysis. Thermal analysis was performed on a simultaneous thermobalance (STA) prototype L81 II (Linseis GmbH, Selb). Samples were heated in corundum crucibles to 600 °C with 3 °C min^{-1} under a dinitrogen atmosphere and then cooled to room temperature.

Preparation of single crystals

$[V^{III}(acac)F_2(py)_2]$ (**1a**), $[V^{III}F_2(py)_4]BF_4$ (**1b**) and $[V^{III}F_3(py)_3]$ (**1d**). The Li_3VF_6 precursor was prepared according to a standard procedure.[6] Absolute pyridine (5–8 mL) was added to the Li_3VF_6 precursor (500–600 mg). The mixture was stirred overnight at 50 °C. The resulting greenish-brown solution was filled into glass tubes positioned in a capped Schlenk tube containing absolute n-pentane or diethyl ether (20 mL). After one to three days, blue-green columns (**1b**), red needles (**1a**), and purple prisms (**1d**) formed.

Analytical data for 1a. NMR: δ_H(400 MHz; CDCl$_3$) 7.1 (2 H, br s, *meta*-H), 7.7 (1 H, br s, *para*-H), 8.6 (2 H, br s, *ortho*-H), 40.7 (1 H, s, CH), 45.6 (3 H, s, Me) and 55.5 (br s, acac). δ_V(105.2 MHz; CDCl$_3$) −850.86. IR: $\tilde{\nu}_{max}$/cm^{-1} 3100–2800w (ν[C–H]$_{py}$), 1605m (ν[C=C]$_{py}$), 1575m (ν[C=O]$_{acac}$, ν[C=C]$_{acac}$),

1530m, 1524s (ν[C=O]$_{acac}$, ν[C=C]$_{acac}$), 1484w (ν[C=C]$_{py}$), 1448s (ν[C=C]$_{py}$), 1376s (ν[C–O]$_{acac}$, γ[C–C]$_{acac}$), 1286w, 1213w, 1067w, 1043m, 766m (γ[C–H]$_{py}$), 702s (γ[C–H]$_{py}$), 638m (γ[C–H]$_{py}$), 578s, 561vs, 537m (ν[V–O], γ[V–acac]), 450m (γ[N$_{py}$–V]), 418w and 330s (ν[V–F]). Anal. found: C, 52.3; H, 5.2; N, 8.2. Calc. for $C_{15}H_{17}F_2N_2O_2V$ (364.25): C, 52.0; H, 4.95; N, 8.1%.

Analytical data for 1b. NMR: δ_H(400 MHz; CDCl$_3$) 7.32 (2 H, br s, *meta*-H), 7.70 (1 H, br s, *para*-H) and 8.63 (2 H, br s, *ortho*-H). δ_V(105.2 MHz; CDCl$_3$) −853.36. IR: $\tilde{\nu}_{max}$/cm^{-1} 3150–2800w (ν[C–H]$_{py}$), 1605s (ν[C=C]$_{py}$), 1483m (ν[C=C]$_{py}$), 1448s (ν[C=C]$_{py}$), 1217m, 1101s, 1058vs, 1043s, 950m, 770m (γ[C–H]$_{py}$), 709m (γ[C–H]$_{py}$), 697s (γ[C–H]$_{py}$), 640m (γ[C–H]$_{py}$), 520w, 499w, 440m (γ[N$_{py}$–V]), 309m (ν[V–F]) and 278m (ν[V–N]). Anal. found: C, 48.95; H, 4.2; N, 11.2. Calc. for $C_{20}H_{20}BF_6N_4V$ (492.14): C, 48.8; H, 4.1; N, 11.4%.

$(pyH)[V^{III}F_2(py)_4]SiF_6$ (**1c**). A saturated solution of the Li_3VF_6 precursor in absolute pyridine was prepared and stirred overnight at 50 °C. After sedimentation of excess material, the overlaying solution was filled into small glass containers that were afterwards sealed with plastic caps. A small hole was drilled into each cap, through which the solvent evaporated slowly. After a few days, light blue crystals formed.

$(pyH)[V^{III}F_4(py)_2]\cdot\frac{2}{3}EtOH$ (**1e**). The standard procedure for the preparation of the Li_3VF_6 precursor was performed with pyridine as solvent. After addition of hydrogen–fluoride solution and stirring the reaction solution for two hours, the excess hydrogen fluoride and one third of the solvent were evaporated under reduced pressure. The residual solution was stored in the refrigerator at −30 °C. After 24 hours, black-green plates formed.

$[Mn^{III}F_2(py)_4][SiF_5(py)]$ (**2a**) and $[Mn^{III}F_3(py)_3]$ (**2b**). A Li_2MnF_5 precursor was prepared from $Mn(OAc)_3\cdot2H_2O$ (Ac: acetyl) according to a standard procedure.[6] It was stirred overnight in absolute pyridine (8 mL) at 50 °C. The resulting orange-brown solution was filled into glass tubes that were positioned in a capped Schlenk tube containing n-pentane or diethyl ether (10 mL). After four days, orange-brown crystals (**2a**) formed. From a few millilitres of the mother liquor stored for five weeks at r.t., orange-brown prisms (**2b**) were obtained.

$[Ni^{II}F_2(py)_4]$ (**3a**). A Li_2NiF_4 precursor was prepared from $[Ni(acac)_2]$ in ethanol according to a standard procedure.[7] Absolute pyridine (5 mL) was added to the Li_2NiF_4 precursor (500–600 mg). The mixture was stirred overnight at 50 °C. The resulting green solution was filled into glass tubes that were positioned in a Schlenk tube filled with n-pentane or diethyl ether (20 mL). After one to three days, light blue crystals (**3a**) formed. After a further few weeks, purple crystals of $[Ni^{II}(acac)_2(py)_2]$ (**3b**) began to grow. Anal. found: C, 58.1; H, 4.9; N, 13.2. Calc. for $C_{20}H_{20}F_2N_4Ni$ (413.09): C, 58.15; H, 4.9; N, 13.6%.

Single-crystal X-ray diffraction

Data were collected at 150.00(10) K using an "Oxford Diffraction Xcalibur S" diffractometer equipped with a goniometer in κ geometry, a "Sapphire 3" CCD-detector, a graphite-monochromated "Enhance" Mo-K_α source (λ = 0.71073 Å) and a

"Cryojet XL" sample cooler. Diffraction images were integrated with CRYSALISPRO.[9] An analytical numeric absorption correction was performed using a multifaceted-crystal model.[10] Structures were solved with SHELXT-2014 using a dual-space method and refined with SHELXL-2014 against F_o^2 data using the full-matrix least-squares algorithm.[11] Non-hydrogen atoms were refined anisotropically; hydrogen atoms were refined isotropically with standard riding-models. Molecular graphics were produced using ORTEP-3 for Windows.[12]

The crystal of $[V^{III}(acac)F_2(py)_2]$ (**1a**) was a merohedral twin of type II by rotation of 180° around [100] in reciprocal space (fraction of second component: 0.291[1]) as discovered by the use of COSET.[13]

The tetrafluoroborate ion in $[V^{III}F_2(py)_4]BF_4$ (**1b**) is disordered over a position of higher symmetry and was treated using enhanced rigid-bond restraints.

The crystal of $(pyH)[V^{III}F_2(py)_4]SiF_6$ (**1c**) was twinned by rotation of −90.5869° around (001) in direct space (fraction of second component: 0.163[2]). Its pyridinium ion is rotationally disordered over a special position and constructed from two symmetry-independent atoms. It was modelled as an occupationally disordered species with C20/N20 occupations of 0.375/0.125 to keep the stoichiometry. The position was chosen because of the possibility of hydrogen bonding. The structure of **1c** contains a void of *ca.* 67 Å³ that was checked for un-modelled electron density by using difference Fourier maps as well as PLATON/SQUEEZE.[14] Neither procedure showed a significant residual.

Structure refinement for $[V^{III}F_3(py)_3]$ (**1d**) did not lead to satisfactory results. Probably because of unresolvable twinning, partial substitutional (solid solution) or rotational disorder of the complex molecules, R factors of the final model were very high, the weighting scheme did not converge to sensible values and large residual electron-density maxima were found at physically unreasonable positions. Therefore, the suggested structure is to be understood as merely modelling connectivity and cell content for the major component.‡

Because the crystal system of $(pyH)[V^{III}F_4(py)_2] \cdot \frac{2}{3}EtOH$ (**1e**) initially seemed to be orthorhombic, an inappropriate data-collection strategy had been chosen resulting in a somewhat lower completeness. In spite of this shortcoming, the structure is of high quality. One pyridinium ion (N50–C52) is rotationally disordered over a special position and constructed from three symmetry-independent atoms. It was modelled as an occupationally disordered species with C50/N50 occupations of 0.5 each to keep the stoichiometry. The position was chosen because of the possibility of hydrogen bonding and the electron density found. The oxygen-borne hydrogen atom was refined with a restrained 1,2-distance (0.84 Å) and $U_{iso}(H60) = 1.2U_{eq}(O60)$. The nitrogen-borne hydrogen atom in the disordered pyridinium ion was fully constrained to the nitrogen atom. The one in the ordered pyridinium ion (N40–C45) was

refined with a restrained 1,2-distance (0.88 Å), a same-1,3-distance restraint and $U_{iso}(H40) = 1.2U_{eq}(N40)$.

The crystal of $[Mn^{III}F_3(py)_3]$ (**2b**) was twinned by rotation of *ca.* 180° around (001) in direct space (fraction of second component: 0.356[3]). Some reflections had to be excluded from the refinement because of problems properly separating them.

CCDC 1063076–1063078 and 1063080–1063083 contain the supplementary crystallographic data for this paper.

Results and discussion

Species from the Li₃VF₆ precursor

The following pyridine adducts of species contained in the Li_3VF_6 precursor were isolated (py: pyridine): $[V^{III}(acac)F_2(py)_2]$ (**1a**), $[V^{III}F_2(py)_4]BF_4$ (**1b**), $(pyH)[V^{III}F_2(py)_4]SiF_6$ (**1c**), $[V^{III}F_3(py)_3]$ (**1d**) and $(pyH)[V^{III}F_4(py)_2] \cdot \frac{2}{3}EtOH$ (**1e**). Because hydrogen fluoride reacts with the glassware used during the precursor synthesis,[6] tetrafluoroborate and hexafluorosilicate are present in the precursor solutions. The diffusion method, as described in the experimental part, yielded crystals of compounds **1a**, **1b** and **1d** that always co-crystallise and are prone to twinning. Crystals of **1c** are formed on slow evaporation of the solvent in air. Cooling crystallisation of **1e** occurred when storing reaction mixtures in pyridine at −30 °C. Crystal data and refinement details for **1a–e** are summarised in Table 1.

In the crystal, $[V(acac)F_2(py)_2]$ (**1a**) forms chains along [010] through dispersive C–H⋯F contacts between fluorido ligands and hydrogen atoms of the acetylacetonato ligand ($d[H\cdots F] \approx$ 2.4 Å). The chains are connected by further C–H⋯F contacts along [10$\bar{1}$] ($d[H\cdots F] \approx$ 2.5 Å) and dispersive aromatic contacts along [101]. The complex is a slightly distorted coordination octahedron with the pyridine ligands in a *trans* arrangement (*cf.* Table 2). In **1b** and **1c**, the $[V^{III}F_2(py)_4]^+$ units adopt a *trans* octahedral coordination geometry, which is only slightly distorted. The pyridine rings in **1b** are not coplanar to the V–N–F coordination planes, but slightly twisted out of the latter, while pairs of diametrically opposed pyridine rings are coplanar (Fig. 1).

The $[V^{III}F_2(py)_4]^+$ and BF_4^- ions in **1b** form a three-dimensional network. **1c** crystallises in a layered structure. In [001] direction, layers of $[V^{III}F_2(py)_4]^+$ units alternate with layers of $[SiF_6]^{2-}$ and pyridinium ions, which are associated by hydrogen bonds. Along [001], the $[SiF_6]^{2-}$ ions are located in channels built by the cations. The V–F bonds in the cationic complexes **1b** and **1c** (*ca.* 1.76 Å) are shorter than in the electroneutral complex **1a** (1.85–1.86 Å). The anionic complex **1e** has the longest V–F bonds of the vanadium species described in this work with up to 1.9229(18) Å (*cf.* Table 2). This trend is easily rationalised by assuming an increasingly effective shielding of the central ion's positive charge by the growing number of negatively charged ligands and, thus, a decrease in the electrostatic attraction per fluorido ligand. For comparison, it should be noted that the V–F distance in VF₃ is 1.94 Å, whereas it varies from 1.89 to 1.97 Å in β-Li₃VF₆.[15,16] In both cases, the octahedral (bridging) F₆ coordination environ-

---

‡Crystal data. C₁₅H₁₅N₃F₃V, M = 345.24, orthorhombic, a = 8.2723(5) Å, b = 12.6821(13) Å, c = 30.6745(19) Å, T = 150.00(10) K, space group *Pbca*, Z = 8.

Table 1 Details of the refinement for **1a–c** and **1e**

Crystal data	$[V^{III}(acac)F_2(py)_2]$ (**1a**)	$[V^{III}F_2(py)_4]BF_4$ (**1b**)	$(pyH)[V^{III}F_2(py)_4]SiF_6$ (**1c**)	$(pyH)[V^{III}F_4(py)_2]\cdot\frac{2}{3}EtOH$ (**1e**)
CCDC no.	1063076	1063077	1063078	1063080
Chemical formula	$C_{15}H_{17}N_2F_2O_2V$	$C_{20}H_{20}BF_6N_4V$	$C_{25}H_{26}F_8N_5SiV$	$C_{49}H_{60}F_{12}N_9O_2V_3$
M_r	346.24	492.15	627.54	1187.88
Crystal system, space group	Monoclinic, $P2_1/c$	Monoclinic, $I2/a$	Tetragonal, $P4/mbm$	Monoclinic, $P2_1/n$
a (Å)	16.4170(14)	14.0214(17)	10.8047(2)	8.4345(6)
b (Å)	8.0367(4)	12.8277(10)	10.8047(2)	31.4088(12)
c (Å)	13.1548(12)	13.4718(17)	12.6865(4)	10.9799(6)
α (°)	90	90	90	90
β (°)	113.588(10)	114.259(14)	90	111.971(7)
γ (°)	90	90	90	90
V (Å^3)	1590.6(2)	2209.1(5)	1481.04(7)	2697.5(3)
Z	4	4	2	2
ρ (g cm^{-3})	1.446	1.480	1.407	1.462
μ (mm^{-1})	0.65	0.51	0.45	0.60
Crystal size (mm^3)	0.54 × 0.12 × 0.06	0.70 × 0.19 × 0.16	0.32 × 0.30 × 0.24	0.59 × 0.39 × 0.18
Data collection				
T_{min}, T_{max}	0.831, 0.971	0.812, 0.932	0.907, 0.937	0.800, 0.912
No. of measured, independent and observed^a reflections	12389, 3116, 2613	4570, 2162, 1487	2574, 2574, 1293	11455, 4725, 3538
R_{int}	0.0654	0.0414	0.1390	0.0448
R_σ	0.0623	0.0652	0.0509	0.0639
$(\sin\theta/\lambda)_{max}$ (Å^{-1})	0.617	0.617	0.616	0.617
Refinement				
R_1 (observed/all)^a	0.0403/0.0543	0.0492/0.0822	0.0508/0.1004	0.0471/0.0720
wR_2 (observed/all)^{a,b}	0.0723/0.0778	0.1096/0.1295	0.1201/0.1325	0.0998/0.1114
S/S'	1.010/1.010	1.101/1.041	0.844/0.844	1.030/1.030
Data/restraints/parameters	3116/0/202	2162/30/165	2574/0/60	4725/3/347
$\Delta\rho_{max}$, $\Delta\rho_{min}$ (e Å^{-3})	0.30, −0.34	0.31, −0.38	0.51, −0.25	0.57, −0.33
Weighting parameters u, v^b	0.0284, 0	0.0516, 0.5074	0.0774, 0	0.0362, 2.2766

^{a} $[I > 2\sigma(I)]$. ^{b} $w = 1/[\sigma^2(F_o^2) + (uP)^2 + vP]$ where $P = (F_o^2 + 2F_c^2)/3$.

Table 2 Selected bond lengths (Å) for **1a–c** and **1e**

	$[V^{III}(acac)F_2(py)_2]$ (**1a**)	$[V^{III}F_2(py)_4]BF_4$ (**1b**)	$(pyH)[V^{III}F_2(py)_4]SiF_6$ (**1c**)	$(pyH)[V^{III}F_4(py)_2]\cdot\frac{2}{3}EtOH$ (**1e**)	
				$[(V1)^{III}F_4(py)_2]^-$	$[(V2)^{III}F_4(py)_2]^-$
V–F	1.8515(17)	1.7658(16)	1.762(3) (2×)	1.8832(19)	1.8876(17)
	1.8603(17)	1.7659(16)		1.8837(19)	1.8876(18)
				1.9170(18)	1.9229(18) (2×)
				1.919(2)	
V–N	2.156(2)	2.145(2)	2.134(3) (2×)	2.161(3)	2.158(3) (2×)
	2.164(2)	2.150(2)		2.171(3)	
V–O	2.011(2)				
	2.015(2)				

ment effectively shields the charge of the central vanadium(III) ion. Examples with vanadium(III) in a pure $F_2(py)_4$ coordination have hitherto been unknown.

However, an example for a compound with a different F_2N_4 coordination environment is the 5,7,12,14-tetramethyldibenzo-[b,i][1,4,7,11]-tetraazacyclodecine complex $[V^{III}(C_{22}H_{23}N_4)F_2]PF_6$ described by Schumann,[17] in which the configuration of the VF$_2$ unit is not yet clarified. Another known compound is the complex $[V^{III}(bipy)F_2]BF_4$ (bipy: 2,2′-bipyridine), in which a vanadium ion is coordinated octahedrally by two *cis*-fluorido and the bidentate 2,2′-bipyridine ligands.[18]

The crystals obtained from **1d** were of insufficient quality to allow more than an assessment of connectivity and cell content for the major component, the $[V^{III}F_3(py)_3]$ molecule, that contains an octahedrally coordinated vanadium ion and assumes a *mer* configuration.‡

$(pyH)[V^{III}F_4(py)_2]\cdot\frac{2}{3}EtOH$ (**1e**) is the only anionic vanadium species isolated from the precursor. The asymmetric unit contains one and a half complex anions differing in the orientation of the pyridine ligands. While the mean planes of the pyridine ligands N10–C15 and N20–C25 are rotated by 56.3(1)° with respect to each other, the rings are coplanar through
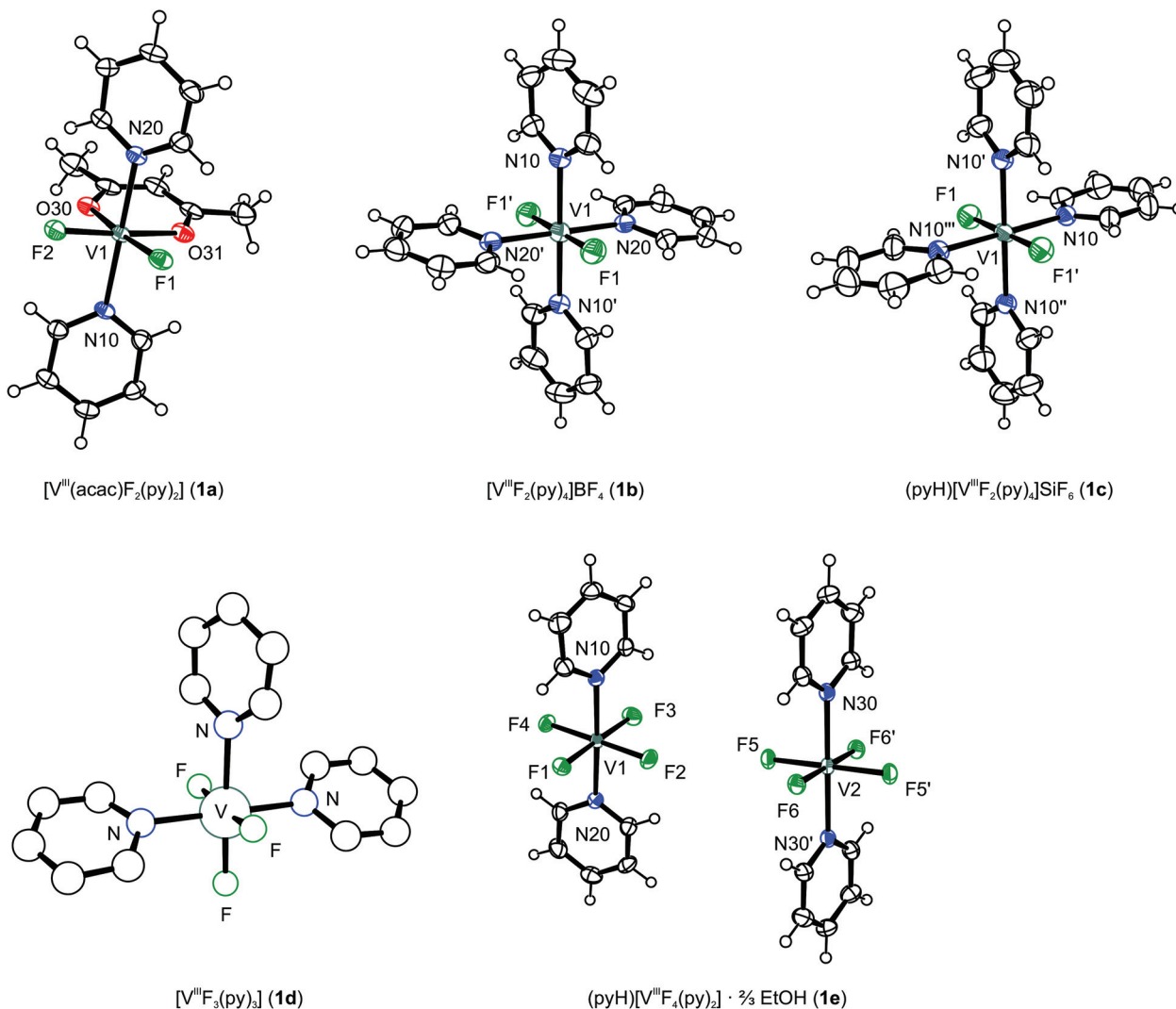
Fig. 1 Molecular structures of vanadium(III) complexes **1a–c**, **1e** (ORTEP representation with ellipsoids of 50% probability; counter ions and solvent molecules omitted for clarity) and connectivity map of **1d** (PLUTON representation).

symmetry in the complex containing N30–C35. The central ions are coordinated in a distorted octahedral fashion by four fluorido and two *trans* arranged pyridine ligands. As regards bond lengths and angles, the complex containing V2 is more symmetric than the one containing V1. The V2 unit interacts with two pyridinium ions (containing N40) *via* hydrogen bonds. Such are also formed between the V1 unit and the ethanol molecule as well as the disordered pyridinium ion containing N50. The packing of the molecules in **1e** can be described as a layered structure parallel to (010). Every layer is built of three sublayers with the sequence V1–V2–V1. Within these sublayers, complexes interact *via* the hydrogen bonds mentioned above.

Species from the Li₂MnF₅ and Li₂NiF₄ precursors

As noted in the introduction, the species [Mn^{III}F₂(py)₄][SiF₅(py)] (**2a**), [Mn^{III}F₃(py)₃] (**2b**) and [Ni^{II}F₂(py)₄] (**3a**) were isolated from

the systems Li–Mn–F and Li–Ni–F and crystallographically characterised (see Table 3). The fluorosilicate anion again is a result of the reaction of hydrogen fluoride with the glassware during precursor synthesis. **3a** has long been known,[19,20] but no crystal structure has been reported so far. The hydrates [Ni^{II}F₂(py)₄]·xH₂O (x = 2 and 7/3) have been known and characterised before.[21,22] From the same mother liquor as **3a**, purple crystals of [Ni^{II}(acac)₂(py)₂] (**3b**) formed after four weeks. This compound has already been reported and both, crystallographically and spectroscopically, characterised.[23–25]

2a forms a structure with alternating layers of [Mn^{III}F₂(py)₄]⁺ and [SiF₅(py)]⁻ ions in (100). The trivalent manganese complex has a nearly undistorted octahedral coordination sphere with the fluorido ligands in a *trans* position (see Fig. 2). The pyridine ligands containing N20 are twisted by 33.6° relative to the N10–V1–F1 plane. At 1.7884(10) Å, the Mn–F bonds (see Table 4) are slightly shorter than those reported for MnF₃ (1.7977–2.1057 Å)[26,27] and MnF₃·3H₂O

Table 3 Details of the refinement for **2a**, **2b** and **3a**

Crystal data	$[Mn^{III}F_2(py)_4][SiF_5(py)]$ (**2a**)	$[Mn^{III}F_3(py)_3]$ (**2b**)	$[Ni^{II}F_2(py)_4]$ (**3a**)
CCDC no.	1063081	1063082	1063083
Chemical formula	$C_{25}H_{25}F_7MnN_5Si$	$C_{15}H_{15}F_3MnN_3$	$C_{20}H_{20}F_2N_4Ni$
M_r	611.53	349.24	413.11
Crystal system, space group	Monoclinic, $C2/c$	Monoclinic, Pc	Monoclinic, $I2/a$
a (Å)	21.4549(11)	15.9240(19)	15.1861(10)
b (Å)	10.3397(5)	8.1630(8)	8.4089(4)
c (Å)	11.9769(7)	12.4914(13)	15.7527(9)
α (°)	90	90	90
β (°)	98.648(5)	102.981(12)	110.717(7)
γ (°)	90	90	90
V (Å^3)	2626.7(2)	1582.2(3)	1881.5(2)
Z	4	4	4
ρ (g cm^{-3})	1.546	1.466	1.458
μ (mm^{-1})	0.62	0.87	1.06
Crystal size (mm^3)	$0.67 \times 0.51 \times 0.28$	$0.45 \times 0.33 \times 0.26$	$1.35 \times 0.62 \times 0.54$
Data collection			
T_{min}, T_{max}	0.778, 0.873	0.747, 0.842	0.480, 0.648
No. of measured, independent and observed^a reflections	5581, 2590, 2331	5530, 5530, 4185	3859, 1839, 1706
R_{int}	0.0192	0.083	0.0149
R_σ	0.0271	0.0726	0.0202
$(\sin \theta/\lambda)_{max}$ (Å^{-1})	0.617	0.617	0.617
Refinement			
R_1 (observed/all)^a	0.0324/0.0385	0.0596/0.0787	0.0247/0.0277
wR_2 (observed/all)^{a,b}	0.0743/0.0768	0.1612/0.1737	0.0642/0.0654
S/S'	1.078/1.078	1.010/1.011	1.056/1.056
Data/restraints/parameters	2590/0/180	5530/2/398	1839/0/124
$\Delta\rho_{max}$, $\Delta\rho_{min}$ (e Å^{-3})	0.26, −0.32	0.49, −0.58	0.24, −0.35
Weighting parameters u, v^b	0.0328, 1.9060	0.1136, 0	0.0302, 0

^{a} $[I > 2\sigma(I)]$. ^{b} $w = 1/[\sigma^2(F_o^2) + (uP)^2 + vP]$ where $P = (F_o^2 + 2F_c^2)/3$.

(1.795(3)–1.856(3) Å).[28] A $[Mn^{III}F_2(py)_4]^+$ species has not previously been described in the literature.

In the group of divalent manganese compounds $[Mn^{II}X_2(py)_4]$, species with X = Cl, Br and I (but not F) are known,[29,30] having a molecular structure similar to **2a**. There are several compounds containing the structure motif $[M^{III}F_2(py)_4]^+$ (M: transition metal), *e.g.*, the chromium compounds $[CrF_2(py)_4]X$ (X = ClO$_4$, Br, I, NO$_3$, PF$_6$)[31,32] and the cobalt compound $[CoF_2(py)_4]ClO_4·\frac{1}{2}H_2O$.[33] Together with **1b** and **1c**, **2a** adds to the hitherto known set of $[M^{III}F_2(py)_4]^+$ species. A special feature of **2a** is the $[SiF_5(py)]^-$ ion. Pyridine fluorosilicates or their polymeric forms have not previously been reported. In contrast, compounds $(NR_4)[SiF_5(NH_3)]$ with R = Me, Et or H exist.[34–36] Furthermore, pyridine adducts of tetrafluorosilane, SiF$_4$·py and SiF$_4$·2py, are known.[37,38] Si–F and Si–N bond lengths in $[SiF_5(py)]^-$ are listed in Table 4. For $(NH_4)[SiF_5(NH_3)]$, the Si–N bond distance is reported to be 1.902(4) Å and is therefore shorter than in **2a**. At 1.6623(15)–1.6703(12) Å, the Si–F bonds in **2a** are somewhat shorter than in $(NH_4)[SiF_5(NH_3)]$ (1.678(1) and 1.680(2) Å). $[Mn^{III}F_3(py)_3]$ (**2b**) and its perdeuterated derivative were described in 1989.[39] The authors reported twinning problems. The single crystals obtained in our experiments were also twinned, but the twin law was found, which allowed for a high-quality refinement of the structure. We found similar cell parameters, but assigned a different space group (Pc instead of $P2_1/c$ as emulated by twinning). The asymmetric unit contains two complexes differing in the orientation of the pyridine ligands with respect to each other and their tilting with respect to the metal–nitrogen bond. In **2b**, both crystallographically independent moieties form layers in (100) connecting symmetry equivalent complexes only through dispersive C–H···F contacts. The layers interact *via* π stacks along [010] to form a three-dimensional network.

The molecular structure of $[Ni^{II}F_2(py)_4]$ (**3a**) is comparable to the $[M^{III}F_2(py)_4]^+$ species discussed before (see Table 4). A distorted octahedral coordination with *trans* aligned fluorido ligands is the basic structural motif. At 2.0061(9) Å, the Ni–F bond length is in the same range as for NiF$_2$ (given as 1.98(1)–2.04(2) Å or 1.997(1)–2.011(1) Å),[40,41] and for the hydrates $[Ni^{II}F_2(py)_4]·2H_2O$ (2.0424(8) Å) and $[Ni^{II}F_2(py)_4]·7/3H_2O$ (2.015(4) Å). The Ni–N bond lengths and coordination angles are also comparable to those in the latter compounds. The molecules of **3a** form chains along *a*, in which the N10-containing pyridine ligands interact *via* π stacks.

Successive flourination of the primary metal precursors

The existence of certain Li$_x$MF$_y$ precursor species can be inferred from the isolation of their solvent adducts. Incorporating $[V^{III}(acac)_2(CH_3CN)_2]BF_4$,[6] the most complete sequence
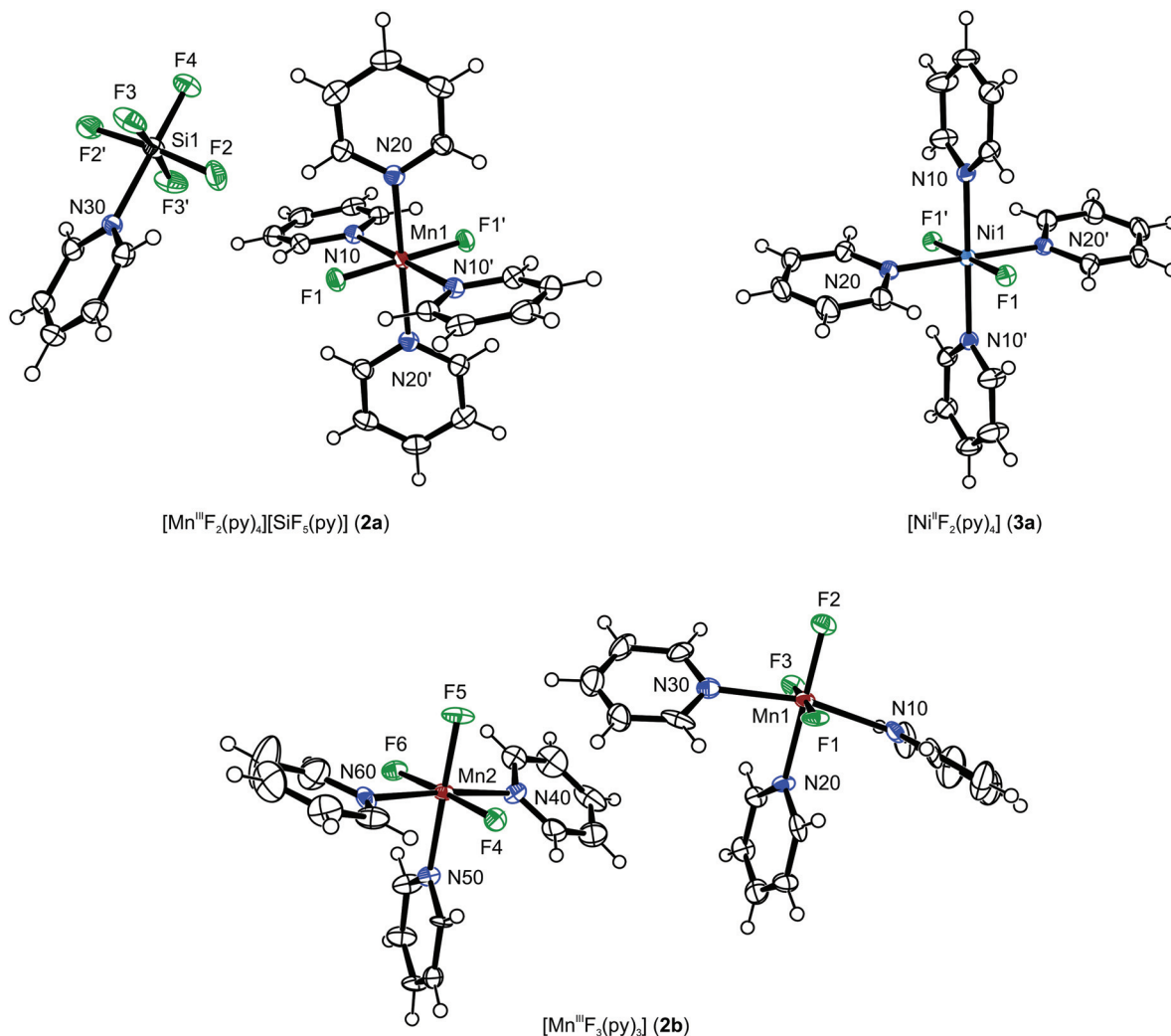
Fig. 2   Molecular structures of manganese(III) complexes **2a–b** and nickel(II) complex **3a** (ORTEP representation with ellipsoids of 50% probability; counter ions omitted for clarity).
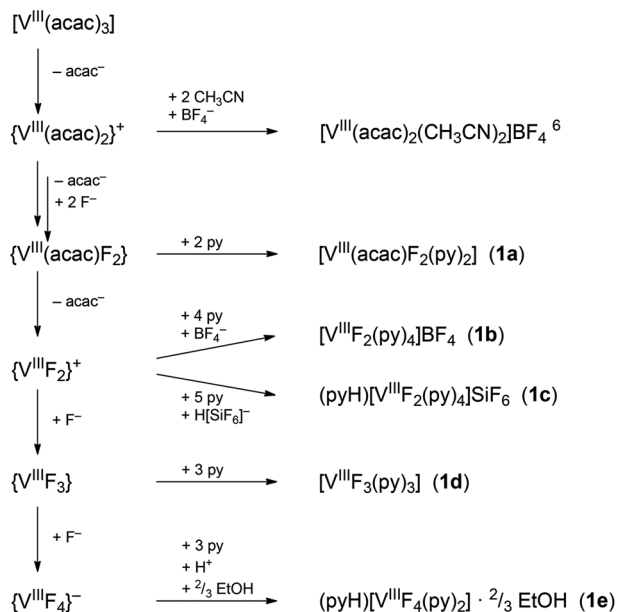
Table 4   Selected bond lengths (Å) for **2a–b** and **3a**

	$[Mn^{III}F_2(py)_4][SiF_5(py)]$ (**2a**) M = Mn	$[Mn^{III}F_3(py)_3]$ (**2b**)		$[Ni^{II}F_2(py)_4]$ (**3a**) M = Ni
		$[(Mn1)^{III}F_3(py)_3]$	$[(Mn2)^{III}F_3(py)_3]$	
M–F	1.7884(10) (2×)	1.811(8) 1.834(8) 1.815(8)	1.815(8) 1.816(8) 1.845(8)	2.0061(9) (2×)
M–N	2.1157(15) (2×) 2.2397(15) (2×)	2.088(11) 2.304(11) 2.331(10)	2.094(11) 2.313(11) 2.323(11)	2.1102(13) (2×) 2.1251(13) (2×)
Si–F	1.6658(11) (2×) 1.6703(12) (2×) 1.6623(15)			
Si–N	2.016(2)			

of fluorination products was found for the Li_3VF_6 precursor. A suitable model for the fluorination of metal acetylacetonates in the precursor-formation process using the example of Li_3VF_6 is shown in Scheme 2. Starting from $[V^{III}(acac)_3]$,

five fluorination steps can be distinguished: first, an acetylacetonato ligand has to be eliminated, leaving behind a cationic $\{V^{III}(acac)_2\}^+$ core as evidenced by the isolation of $[V^{III}(acac)_2(CH_3CN)_2]BF_4$ and $[V^{III}(acac)_2F]$.[6,42] After elimination

$[V^{III}(acac)_3]$

$\downarrow$ $-$ acac$^-$

$\{V^{III}(acac)_2\}^+$ $\xrightarrow[\text{+ BF}_4^-]{\text{+ 2 CH}_3\text{CN}}$ $[V^{III}(acac)_2(CH_3CN)_2]BF_4$ [6]

$\downarrow$ $-$ acac$^-$
$\quad$ $+$ 2 F$^-$

$\{V^{III}(acac)F_2\}$ $\xrightarrow{\text{+ 2 py}}$ $[V^{III}(acac)F_2(py)_2]$ (**1a**)

$\downarrow$ $-$ acac$^-$

$\{V^{III}F_2\}^+$ $\xrightarrow[\text{+ BF}_4^-]{\text{+ 4 py}}$ $[V^{III}F_2(py)_4]BF_4$ (**1b**)

$\xrightarrow[\text{+ H[SiF}_6]^-]{\text{+ 5 py}}$ $(pyH)[V^{III}F_2(py)_4]SiF_6$ (**1c**)

$\downarrow$ $+$ F$^-$

$\{V^{III}F_3\}$ $\xrightarrow{\text{+ 3 py}}$ $[V^{III}F_3(py)_3]$ (**1d**)

$\downarrow$ $+$ F$^-$

$\{V^{III}F_4\}^-$ $\xrightarrow[\text{+ }^2/_3 \text{ EtOH}]{\substack{\text{+ 3 py} \\ \text{+ H}^+}}$ $(pyH)[V^{III}F_4(py)_2] \cdot {}^2/_3 EtOH$ (**1e**)

Scheme 2 Stepwise fluorination of [V(acac)$_3$] and formation of the isolated complexes.

of another acetylacetonato ligand and further fluorination, a $\{V^{III}(acac)F_2\}$ core is formed, which has been trapped in **1a**. Neither $[V^{III}(acac)F_2]$ nor $[V^{III}(acac)F_2(py)]$ have been described in the literature so far. The $\{V^{III}(acac)F_2\}$ core reacts with two more equivalents of HF, forming $\{VF_3\}$ and finally $\{VF_4\}^-$, which were trapped in **1d** and **1e** as shown in Scheme 2.

When the starting materials $[V^{III}(acac)_3]$ and LiOtBu are reacted with hydrogen–fluoride solution, increasingly more highly fluorinated species (up to $\{VF_4\}^-$) are formed within a chemical equilibrium. Although an excess of hydrogen fluoride is used, exhaustive fluorination is not accomplished.

The question remains how Li$_3$VF$_6$ is formed during the decomposition of the inhomogeneous precursor material. For precursor synthesis, LiOtBu and $[V^{III}(acac)_3]$ are reacted in the ratio 3 : 1 with an excess of HF to achieve a stoichiometry of F$_6$Li$_3$V. However, the precursor can neither be Li$_3$VF$_6$ nor a stoichiometric mixture of LiF and VF$_3$, as elemental analysis shows carbon, hydrogen and oxygen to be present in considerable amounts. During precursor decomposition, the following steps occur: while heating, residual solvent evaporates and is carried away by the gas flow. In general, at about 200 °C, acetylacetonates start to decompose;[43] pure $[V^{III}(acac)_3]$ was reported to decompose at about 250 °C.[44] To avoid oxidation, working under a dinitrogen atmosphere is necessary. Under these conditions, organic residues are carbonised, giving rise to the black colour of the Li$_3$VF$_6$ material and its residual carbon content. Before reaching 300 °C, the decomposition of Li$_2$SiF$_6$ to LiF and SiF$_4$ starts. Gaseous SiF$_4$ is also carried away by the gas flow. Normally, the decomposition of Li$_2$SiF$_6$ should occur at higher temperature as reported in the literature: at 290 °C[45]
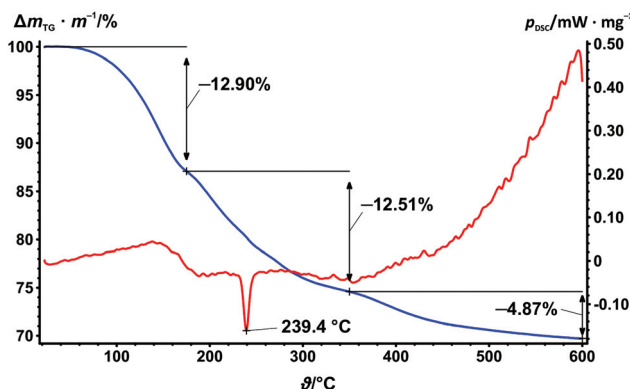

Fig. 3 TG/DSC during decomposition of the Li$_3$VF$_6$ precursor (synthesised in EtOH) in a dinitrogen atmosphere. Blue curve: TG signal, red curve: DSC signal, black arrows: mass changes. $\Delta m_{TG}\, m^{-1}$/%: mass loss in per cent.
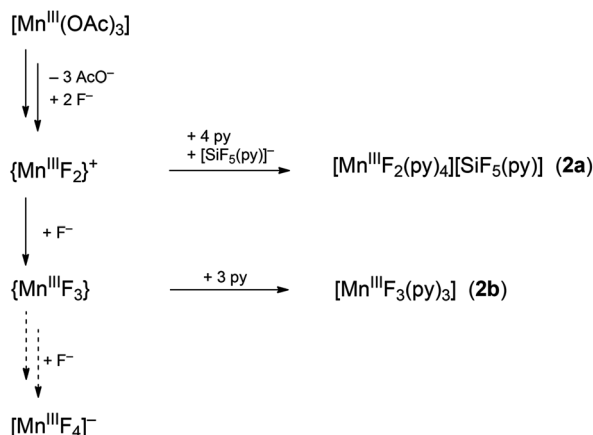
or 350–370 °C[46] in dry air. We have not found any Li$_2$SiF$_6$ in Li$_3$VF$_6$ precursor samples prepared under dinitrogen at 300 °C. This indicates that the decomposition of Li$_2$SiF$_6$ occurs at lower temperatures under precursor decomposition conditions as compared to pure samples. To substantiate this, a sample of pure Li$_2$SiF$_6$ prepared from Li$_2$CO$_3$ and aqueous H$_2$SiF$_6$ was calcined for four hours at 240 °C under dinitrogen flow. X-ray powder diffraction showed that the product was a mixture of Li$_2$SiF$_6$ and LiF. At 300 °C, the formation of monoclinic β-Li$_3$VF$_6$ as the main component is observed, so that the decomposition of the fluorinated species and their reaction with LiF can be assumed.

To verify this concept, the precursor decomposition was investigated by thermogravimetry (TG) and differential scanning calorimetry (DSC, see Fig. 3). The sample loses 12.9% of its mass up to 180 °C. This is in the temperature range of a possible solvent loss. Between 180 and 350 °C, the sample loses another 12.5% of its mass, while acetylacetonate and Li$_2$SiF$_6$ decompose. From 233 to 250 °C, a DSC signal for an exothermic process appears with its maximum at about 239 °C. As the precursor contains a plethora of species, which can react with each other during decomposition, we have unfortunately been unable to clarify the origin of this signal. However, we have ruled out the decomposition of Li$_2$SiF$_6$ or acetylacetonate compounds (*e.g.*, [V(acac)$_3$]), because these processes are known to be endothermic.[44,47]
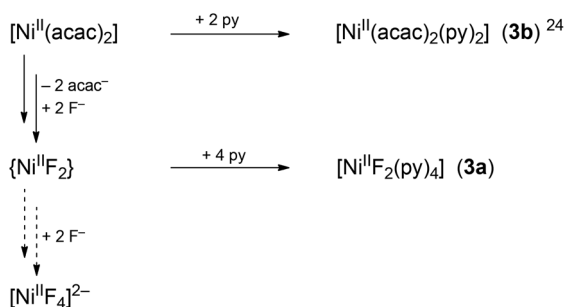
Upon reaching the final temperature of 600 °C, the sample had lost a total of 30.3% of its mass. This value is in the typical range of losses observed during decomposition (25–40% for Li$_3$VF$_6$ precursors).

It is safe to assume that similar processes occur with Li$_2$MnF$_5$ and Li$_2$NiF$_4$ precursors. In the system Li–Mn–F, $\{MnF_2\}^+$ and $\{MnF_3\}^+$ were captured—in analogy to the system Li–V–F (see Scheme 3). Species with the core $\{Mn^{III}F_x\}^{(x-3)-}$ have not been found so far for $x = 4$ and 5. In the system Li–N–F, [Ni(acac)$_2$] partly reacts with hydrogen fluoride to form NiF$_2$, as indicated by the presence of **3a** (see Scheme 4). It is as yet

$[Mn^{III}(OAc)_3]$

$\downarrow$ − 3 AcO⁻ + 2 F⁻

$\{Mn^{III}F_2\}^+$ $\xrightarrow{+ 4\ py\ +\ [SiF_5(py)]^-}$ $[Mn^{III}F_2(py)_4][SiF_5(py)]$ **(2a)**

$\downarrow$ + F⁻

$\{Mn^{III}F_3\}$ $\xrightarrow{+ 3\ py}$ $[Mn^{III}F_3(py)_3]$ **(2b)**

$\downarrow$ + F⁻

$[Mn^{III}F_4]^-$

Scheme 3 Stepwise fluorination of $[Mn(OAc)_3]$ and formation of the isolated complexes.

$[Ni^{II}(acac)_2]$ $\xrightarrow{+ 2\ py}$ $[Ni^{II}(acac)_2(py)_2]$ **(3b)** [24]

$\downarrow$ − 2 acac⁻ + 2 F⁻

$\{Ni^{II}F_2\}$ $\xrightarrow{+ 4\ py}$ $[Ni^{II}F_2(py)_4]$ **(3a)**

$\downarrow$ + 2 F⁻

$[Ni^{II}F_4]^{2-}$

Scheme 4 Stepwise fluorination of $[Ni(acac)_2]$ and formation of the isolated complexes.

unknown if anionic fluoridometal species exist in these systems. Finally, Li_2MnF_5 and Li_2NiF_4 will be formed when the mixture of transition-metal species and LiF is heated under dinitrogen flow.

Conclusions

The results presented above give detailed insight into the processes of the fluorolytic sol–gel synthesis of ternary lithium transition-metal fluorides. After stabilising precursor species with pyridine and growing single crystals from the pyridine solutions, it became apparent that the precursor is a mixture of transition-metal compounds with different degrees of fluorination. On the basis of these results, previous analytical data from X-ray diffraction and spectroscopic methods may be better understood. In the case of the synthesis of Li_3VF_6 starting from $[V^{III}(acac)_3]$, four fluorination steps were identified by isolating and characterising the pyridine adducts **1a–e**. Further experiments with Li_2MnF_5 and Li_2NiF_4 precursors led to the species **2a–b** and **3a**. In addition, first attempts to isolate species from the system Li–Fe–F already indicate the presence of $[Fe^{III}F_2(py)_4]BF_4$. This demonstrates that the conclusions made for Li_3VF_6 are transferable to the fluorolytic sol–gel syn-

thesis of other ternary fluorides in general. The elucidation of these processes is necessary for further research on the notoriously low yields of Li_2MnF_5 and Li_3FeF_6, as well as the reduction occurring in these systems. As mentioned in the introduction, Li_2MnF_5 and Li_3FeF_6 were invariably obtained together with the difluorides MF_2. The question, whether divalent species are already formed during precursor synthesis, is important for addressing this issue. Stabilisation with additional solvent ligands such as pyridine is a promising method to help clarify these open questions.

Acknowledgements

Notes and references

1 J. Koyama, I. Tanaka and H. Adachi, *J. Electrochem. Soc.*, 2000, **147**, 3633.

2 E. Gonzalo, A. Kuhn and F. Garcia-Alvarado, *J. Power Sources*, 2010, **195**, 4990.

3 A. Basa, E. Gonzalo, A. Kuhn and F. Garcia-Alvarado, *J. Power Sources*, 2012, **207**, 160.

4 I. Gocheva, K. Chihara, S. Okada and J. Yamaki, *Proceedings of the Lithium Battery Discussions 2011 – Electrode Materials*, Arcachon, France, 2011.

5 E. Kemnitz, U. Groß, S. Rüdiger and C. S. Shekar, *Angew. Chem., Int. Ed.*, 2003, **115**, 4383.

6 J. Kohl, D. Wiedemann, S. Nakhal, P. Bottke, N. Ferro, T. Bredow, E. Kemnitz, M. Wilkening, P. Heitjans and M. Lerch, *J. Mater. Chem.*, 2012, **22**, 15819.

7 J. Kohl, S. Nakhal, N. Ferro, P. Bottke, M. Wilkening, T. Bredow and M. Lerch, *Z. Anorg. Allg. Chem.*, 2013, **639**, 326.

8 A. Dimitrov, J. Koch, S. I. Troyanov and E. Kemnitz, *Eur. J. Inorg. Chem.*, 2009, **35**, 5299.

9 Agilent Technologies, *CrysAlisPro Software System, version 171.37*, Agilent Technologies Ltd., Oxford, UK, 2014.

10 R. C. Clark and J. S. Reid, *Acta Crystallogr., Sect. A: Fundam. Crystallogr.*, 1995, **51**, 887.

11 G. M. Sheldrick, *Acta Crystallogr., Sect. A: Fundam. Crystallogr.*, 2008, **64**, 112.

12 L. J. Farrugia, *J. Appl. Crystallogr.*, 2012, **45**, 849.

13 P. Boyle, *J. Appl. Crystallogr.*, 2014, **47**, 467–470.

14 P. van der Sluis and A. L. Spek, *Acta Crystallogr., Sect. A: Found. Crystallogr.*, 1990, **46**, 194.

15 W. Massa, *Z. Kristallogr.*, 1980, **153**, 201.

16 K. H. Jack and V. Gutmann, *Acta Crystallogr.*, 1951, **4**, 246.

17 H. Schumann, *Polyhedron*, 1996, **15**, 845.

18 S. J. Kavitha, K. Panchanatheswaran, J. N. Low and C. Glidewell, *Acta Crystallogr., Sect. E: Struct. Rep. Online*, 2005, **61**, m1965.

19 I. I. Kalinichenko and A. A. Knyazeva, *Dokl. Akad. Nauk SSSR*, 1966, **169**, 887.

20 A. A. Knyazeva, I. I. Kalinichenko and T. A. Degtyareva, *Zh. Neorg. Khim.*, 1967, **12**, 1213.

21 J. Holzbock, W. Sawodny and L. Walz, *Z. Kristallogr.*, 1997, **212**, 115.

22 P. Halasyamani, M. J. Willis, C. L. Stern and K. R. Poeppelmeier, *Inorg. Chim. Acta*, 1995, **240**, 109.

23 J. T. Hashagen and J. P. Fackler, *J. Am. Chem. Soc.*, 1965, **87**, 2821.

24 R. C. Elder, *Inorg. Chem.*, 1968, **7**, 2316.

25 K. Nakamoto, C. Udovich and J. Takemoto, *J. Am. Chem. Soc.*, 1970, **92**, 3973.

26 F. Schrötter and B. G. Müller, *Z. Anorg. Allg. Chem.*, 1993, **619**, 1426.

27 M. A. Hepworth and K. H. Jack, *Acta Crystallogr.*, 1957, **10**, 345.

28 M. Molinier and W. Massa, *J. Fluorine Chem.*, 1992, **57**, 139.

29 M. A. Araya, F. A. Cotton, J. H. Matonic and C. A. Murillo, *Inorg. Chem.*, 1995, **34**, 5424.

30 C. J. H. Jacobsen, E. Pedersen, J. Villadsen and H. Weihe, *Inorg. Chem.*, 1993, **32**, 1216.

31 J. Glerup, J. Josephsen, K. Michelsen, E. Pedersen and C. E. Schäfer, *Acta Chem. Scand.*, 1970, **24**, 247.

32 G. Fochi, J. Strähle and F. Gingl, *Inorg. Chem.*, 1991, **30**, 4669.

33 G. Glerup, C. E. Schäffer and J. Springborg, *Acta Chem., Scand. Ser. A*, 1978, **32**, 673.

34 I. Wharf and M. Onyszchuk, *Can. J. Chem.*, 1972, **50**, 3450.

35 H. C. Clark, K. R. Dixon and J. G. Nicholson, *Inorg. Chem.*, 1969, **8**, 450.

36 C. Plitzko and G. Meyer, *Z. Anorg. Allg. Chem.*, 1996, **622**, 1646.

37 E. L. Muetterties, *J. Am. Chem. Soc.*, 1960, **82**, 1082.

38 V. A. Bain, R. C. Killean and M. Webster, *Acta Crystallogr., Sect. B: Struct. Crystallogr. Cryst. Chem.*, 1969, **25**, 156.

39 W. Sawodny, K. N. Rau and W. Bolkart, *J. Fluorine Chem.*, 1989, **43**, 119.

40 J. W. Stout and S. A. Reed, *J. Am. Chem. Soc.*, 1954, **76**, 5279.

41 M. M. Costa, J. A. Paixão, M. J. de Almeida and L. C. Andrade, *Acta Crystallogr., Sect. B: Struct. Sci.*, 1993, **49**, 591.

42 M. K. Chaudhuri and S. K. Ghosh, *Inorg. Chem.*, 1984, **23**, 2367.

43 J. von Hoene, R. G. Charles and W. M. Hickam, *J. Phys. Chem.*, 1958, **62**, 1098.

44 G. A. M. Hussein, *Thermochim. Acta*, 1995, **256**, 347.

45 Y. N. Moskvich, B. I. Cherkasov and G. I. Dotsenko, *Zh. Strukt. Khim.*, 1979, **20**, 348.

46 D. L. Deadmore, J. S. Machin and A. W. Allen, *J. Am. Ceram. Soc.*, 1962, **45**, 120.

47 R. R. Patil, M. Rujuta Barve, M. S. Kulkarni, B. C. Bhatt and S. V. Moharil, *Phys. B*, 2012, **407**, 629.